



COMPUTATIONAL INVESTIGATION INTO THE EFFECT OF PITCH RATIOS ON B-SERIES PROPELLER PERFORMANCE

Ahmad Fitriadhy^{1,*}, Nur Amira Adam² and Anuar Abu Bakar³

¹Program of Naval Architecture, Faculty of Ocean Engineering Technology and Informatics, Universiti Malaysia Terengganu, Kuala Terengganu, Terengganu, Malaysia. naoe.afit@gmail.com

²School of Port, Logistics and Management, Netherlands Maritime University College, Johor, Malaysia. amiraadam.nur@gmail.com

³Program of Naval Architecture, Faculty of Ocean Engineering Technology and Informatics, Universiti Malaysia Terengganu, Kuala Terengganu, Terengganu, Malaysia. anuarbakar@umt.edu.my

Abstract:

This study presents Computational Fluid Dynamics (CFD) simulation to predict the thrust coefficient (K_T), torque coefficient (K_Q) and efficiency (η) in open-water conditions. The effect of various pitch ratio (P/D) and blade number (Z) for the type of B-series have been appropriately taken into account in the computational simulation. In general, the results revealed that the higher value of advance ratio leads to decrease the values of K_T and K_Q coefficients. In addition to the propeller's efficiency, it proportionally increases with respect to the advance number (J); then it adequately decreases at $J > 0.8$. It should be noted here that the subsequent increase of propeller pitch ratio within the range of $0.6 \leq P/D \leq 1.3$ is proportional to the values of K_T , K_Q and η . This can be explained by the fact that the increase of pitch ratio resulted in the increase of the scalar torque and static pressure. Meanwhile, the propeller with $P/D = 1.3$ produces the highest efficiency by 81.2% at $J=1.15$. Furthermore, the propeller with five blade number ($Z=5$) has the lowest propeller efficiency, which occurred due to increase of the projected blade area. Merely, the current computational result is very useful for acquiring a fundamental understanding of the propeller quantities, especially in open-water conditions.

Keywords: CFD, pitch ratio, efficiency, propeller, thrust coefficient, torque coefficient.

NOMENCLATURE

K_Q	torque coefficient
K_T	thrust coefficient
J	advance number
Z	blade number

P/D | pitch ratio
Greek symbols

ρ	density
ν	kinematic viscosity
η	efficiency

1. Introduction

Geometrically, a propeller has been designed as rotational blades incorporated with pitch angle to create a pressure difference between the two surfaces i.e., trailing, and leading edges. This rotating propeller presented in the form of helical spiral flow will inherently produce thrust that is ultimately able to propel a ship. Basically, the propellers can be primarily categorized into two pitch types i.e., fixed pitch propeller (FPP) and controllable pitch propeller (CPP). Referring to Dymarski (2008), the CPP was found to have higher efficiency in the wide range of velocities and more suitable to increase the ship's maneuverability. However, CPP has higher initial cost and complex installation process of the pitch control mechanism in the hub. In addition, the FPP geometry is deemed more dependable, exhibiting favorable efficiency values under the design condition, easier to install and has lower maintenance cost compared to CPP at the stipulated operating condition (Bacciaglia *et al.*, 2020).

Several researchers have investigated the hydrodynamics performance of FPP through theoretical and experimental approaches. Yousefi *et al.* (2023) conducted experiments and found that the thrust and torque coefficients increase with the increasing of propeller pitch ratio. Rahman *et al.* (2017) proposed the theoretical method using lifting line theory and lifting surface correction factors shows that the decrease of the thrust value represents the reduction of the camber-chord ratio. Meanwhile, Abbasi *et al.* (2018) has stated that the thrust and torque coefficients are reduced by increasing the angle of flow and increasing the advance coefficient. Mao and Young (2016) reported that the pitch, yaw-pitch, and pitch-sway damping was proportional increase of the propeller's skew. The propeller performance on various tip rake propellers have been performed by Kang *et al.*

(2019), the study shows that the efficiency value for backward tip rake propeller was slightly less compared with forward tip rake propellers. Lastly, Adam et al. (2020) concluded that a higher blade number significantly influences propeller performance compared to other factors. Referring to our literature survey, various propeller configurations have been considered. Thus, the study to predict the propeller performance of FPP geometry at various pitch conditions is obviously necessary.

In the presents study, a computational investigation into the effect of various pitch ratios on B-series propellers performance has been appropriately conducted in open-water conditions. To achieve the objective, the authors employ the CFD simulation approach enabling capture of dynamic flow characteristics and interactions surrounding the blade, ensuring a comprehensive understanding of the propeller's behavior and prevent low efficiency. The CFD approach has effectively demonstrated the accuracy of its model through validation with experimental results, Adam *et al.* (2020). This computational analysis includes crucial parameters such as thrust coefficient (K_T), torque coefficient (K_Q), and efficiency (η). The CFD software Numeca Fine™/Turbo is employed for mesh creation, fluid dynamics simulation, and result analysis. Utilizing a solver based on the 3D Reynolds-Averaged Euler and Navier-Stokes equations, Fine™/Turbo is adept at simulating internal, rotating, and turbomachinery flows across diverse fluid types. Additionally, CFD simulations are extended to scrutinize propeller performance, considering various pitch ratios and blade numbers. The outcomes, including K_T , K_Q , and η coefficients, are thoroughly discussed and illustrated through scalar torque and static pressure distributions around the propeller blades.

2. Theoretical Background

2.1 Conservation equation

Engaging in CFD simulation entails basic mathematical expressions that govern continuity, momentum, and the preservation of energy. Eq.(1) illustrates the mass continuity equation in conservation form, which depends on the stability and constant density of incompressible flows. Here, ρ signifies density and U_i represents the velocity vector's averaged Cartesian components (Prakash and Nath, 2002).

$$\frac{\partial \rho}{\partial t} + \frac{\partial}{\partial x_i} (\rho u_i) = 0 \quad (1)$$

As a fluid element undergoes motion, its net force is the result of multiplying its mass by acceleration. Eq.(2), the overarching Navier-Stokes equation, applies the concept of linear momentum conservation. Here, P represents static pressure, g_i denotes gravitational acceleration, F_i denotes an external body force acting on the averaged velocity vector in Cartesian components in the i^{th} direction ($i=1,2,3$) and δ_{ij} is the Kronecker delta, equal to unity when i equals j and zero when i is not equal to j .

$$\frac{\partial}{\partial t} (\rho u_i) + \frac{\partial}{\partial x_i} (\rho u_i u_i) = -\frac{\partial P}{\partial x_i} + \frac{\partial \tau_{ij}}{\partial x_j} + \rho g_i + F_i \quad (2)$$

2.2 Turbulence model

In this scenario, we employ the Spalart-Allmaras transport equation model to compute the propeller's rotating motions. This turbulence model is configured to capture variations in the speed and direction of the flow through algebraic models (Deck et al., 2002; Lorin et al., 2006; Hejlesen et al., 2012). For external flow applications, the kinematic turbulent viscosity $\nu_t (m^2/s)$ in this model can be prescribed and calculated based on the assumption, $\frac{\nu_t}{\nu} = 1$ (Kostic, 2015). Eq.(3) expresses the model governing the transport of the specified variable.

$$\frac{\partial \tilde{\nu}}{\partial t} + \frac{\partial \rho u_j \tilde{\nu}}{\partial x_j} = \frac{\partial}{\partial x_j} \left[\left(\mu + \frac{\mu_\tau}{\sigma} \right) \frac{\partial \tilde{\nu}}{\partial x_j} \right] + c_{b2} \frac{\partial \tilde{\nu}}{\partial x_j} \frac{\partial \rho \tilde{\nu}}{\partial x_i} + c_{b1} \rho \tilde{W} \tilde{\nu} - c_{w1} f_w \rho \left(\frac{\tilde{\nu}}{y} \right) \quad (3)$$

Eqs.(4) and (5) define the eddy viscosity and damping function, respectively..

$$\mu_\tau = f_{v1} \rho \tilde{\nu} \quad (4)$$

$$f_{v1} = \frac{X^3}{X^3 + c_{v1}^3} \quad (5)$$

where, $X = \frac{\bar{v}}{v}$ with $v = \mu/\rho$.

2.3 Rotating section (Angle Attack)

In this section, each blade of the propeller composes of various pitch angles, which define the different distance of propeller rotating in one revolution without considering the slip (International (2009) and Gerr (1989)). The value of pitch angle is the trigonometric ratio and the angle of blades to rotate in anti-clockwise direction that can be written below:

$$\theta = \tan^{-1} \left(\frac{Pitch}{2\pi r} \right) \tag{6}$$

where r is the distance from propeller’s tip to the hub (m).

2.4 Propeller hydrodynamic characteristics

Testing the propeller model in an open-water scenario evaluates its performance independently of the ship's resistance. Although the thrust (T) and torque (Q) quantity already computed in CFD, the evaluation results required a non-dimensional value such as K_T , K_Q and η coefficients to illustrated in graph with respect to the advance ratio (J) (Ozturk *et al.*, 2022). Here, the water advance velocity will be represented in advance ratio as demonstrated in Eq.(7):

$$J = \frac{v_a}{nD} \tag{7}$$

The propeller efficiency given in Eq. (8) clearly showed that the thrust and torque coefficients are an important input value that can be obtained by using Eqs. 9 and 10.

$$\eta = \frac{J K_T}{2\pi K_Q} \tag{8}$$

$$K_T = \frac{T}{\rho n^2 D^4} \tag{9}$$

$$K_Q = \frac{Q}{\rho n^2 D^5} \tag{10}$$

3. Simulation Condition

3.1 Propeller data

Table 1 clearly presents the primary dimension of the right-handed propeller. Three-dimensional representation of the propeller and its pitch ratios are depicted in Fig. 1.

Table 1: The existing principal data of propeller

Geometry	Dimension	
	Actual	Model
Diameter (mm)	3650	119.25
AE/AO	0.695	
P/D	1.0	
Blade Number	4	
Scale	1:30.6	

3.2 Parametric studies

In the current CFD simulation, the effect of the different pitch ratios and numbers of blade from P/D = 0.6 to 1.3 have been employed as summarized in Table 2. Here, the number of blades of Z = 4 is set to be constant and the advance ratio has been applied within the range $0.1 \leq J \leq 1.30$ in condition 1. Meanwhile, the J = 0.5 and 1200

RPM is set to be constant in condition 2. This is due to an optimum pitch ratio which leads to better propeller performance in designed condition.

Table 2: Parametric studies of computational simulations

P/D	Condition 1	Condition 2		
	RPM	Number of Blade (Z)		
	1200 RPM	Z = 3	Z = 4	Z = 5
0.6	√	√	√	√
0.7	√	√	√	√
0.8	√	√	√	√
0.9	√	√	√	√
1.0	√	√	√	√
1.1	√	√	√	√
1.2	√	√	√	√
1.3	√	√	√	√

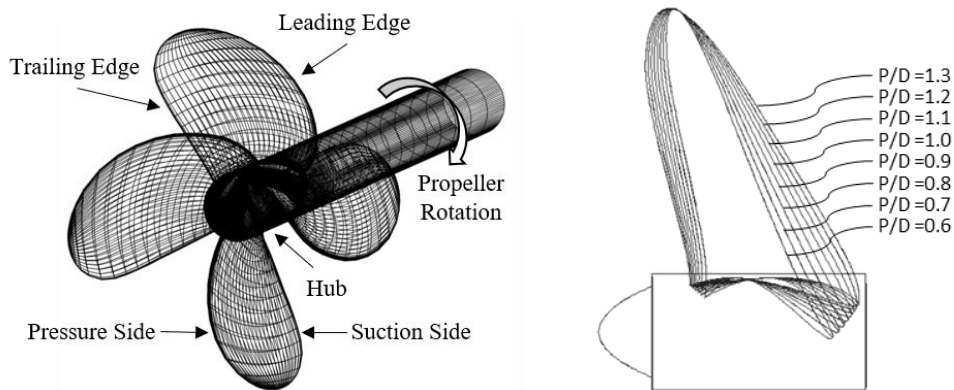


Fig. 1: Propeller geometry (left) and pitch ratio values (right)

3.3 Computational domain and mesh generation

Initially, the pitch angle is set on the Computer-Aided Design (CAD) software, which is eventually imported into the CFD software called Numeca Fine™/Turbo. Simulating the performance of a propeller at various pitch ratios in open-water case is set up. Here, the block and boundary of the blade are duplicated along a designated axis over a specified angle. This intentional duplication is aimed at reducing computational time (Colley, 2012).

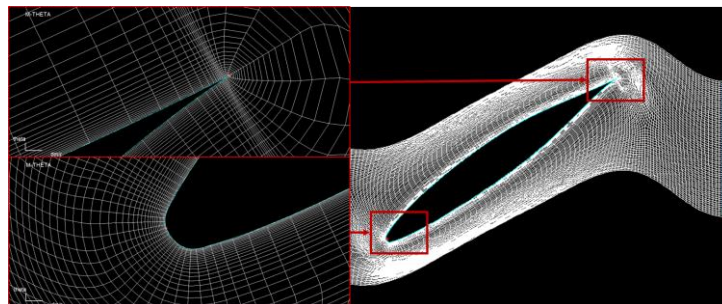


Fig. 2: Local mesh refinement

In meshing, we chose curvilinear streamwise 04H grid arrangement with 97 points along the pitchwise direction (Numeca User manual, 2009). The propeller mesh had around 2.8 million nodes, with an initial cell size of 1.0 μm for blades and hub surfaces. To boost accuracy, we applied local mesh refinement, reducing grid size to capture significant pressure gradients near the blade wall, as shown in Fig. 2.

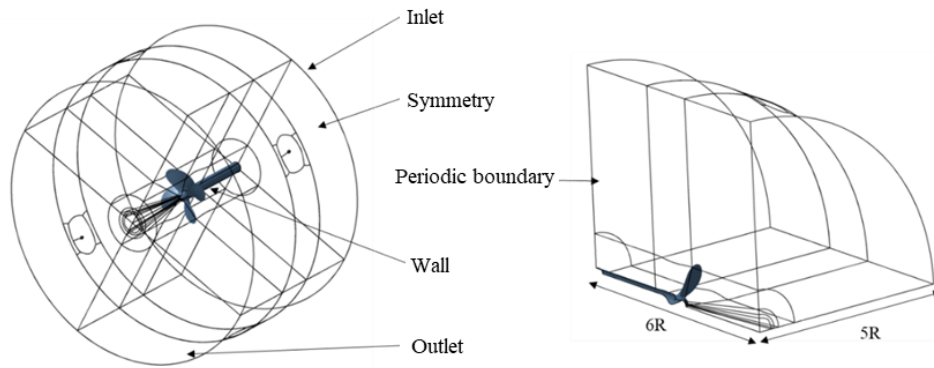


Fig. 3: Boundary conditions

The inlet maintains a constant flow velocity, while the outlet has a static pressure, as depicted in Fig. 3. Solid boundary conditions for propeller revolution consider fixed fluid velocity, adhering to a right-handed propeller orientation (Numeca User manual, 2009). Due to the computational complexity of the fluid dynamics challenge, the Merkle preconditioning method is applied to enhance the speed of reaching a solution and optimize performance, especially at low flow speeds, following recommendations by Martinez et al. (2015) and Folkner (2013). Meshing sensitivity studies, detailed in Table 3, determine the optimal number of cells for stability in computational results. The convergence analysis demonstrates monotonic convergence ($R_i = 0.34$), as per Eq. (11) (ITTC, 2017).

$$R_i = \varepsilon_{i,21} - \varepsilon_{i,32} \quad (11)$$

where $\varepsilon_{i,21} = \hat{S}_{i,2} - \hat{S}_{i,1}$ between medium-fine and $\varepsilon_{i,32} = \hat{S}_{i,3} - \hat{S}_{i,2}$ for course-medium that used to define the convergence ratio. The $\hat{S}_{i,1}, \hat{S}_{i,2}, \hat{S}_{i,3}$ determine convergence condition correspond to solution with fine, medium and coarse input parameter, respectively (Wald, 2006). Hence, the selection for 2,817,090 meshing cells (case B) proved sufficient for whole simulations, offering more effective computational times compared to the unnecessary 4,000,666 cells.

Table 3: Study of mesh independence at various numbers of cell meshing

Case	J	Meshing Numbers	10K _Q	K _T	η
A	0.5	1,789,042	0.44371	0.27545	0.49402
B		2,817,090	0.43853	0.27450	0.49821
C		4,000,666	0.43875	0.27616	0.50089

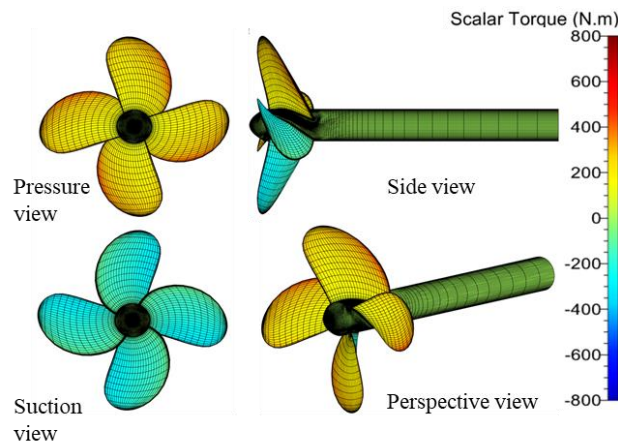


Fig. 4: Magnitude of scalar torque for J = 0.5 and RPM = 1200

In the CFD simulation's final stage, CFView™ produces graphical results for scalar torque and static pressure (Fig. 4). With an appropriate total mesh count, the initial validation aligns well with experimental tests (Table 4), showing acceptable percentage discrepancies: approximately 1.04% for K_T, 2.24% for K_Q, and 1.23% for η.

Table 4: CFD simulations and experiments corresponding Z=4 and RPM=1200

J	K_T			$10K_Q$			η		
	CFD	EXP	(%)	CFD	EXP	(%)	CFD	EXP	(%)
0.5	0.274	0.277	-1.040	0.438	0.448	-2.238	0.498	0.492	1.226
0	5	4		5	5		2	0	

*The negative sign (-) indicates that the CFD simulation result is below the model test result.

4. Results and Discussion

Propeller performance analyses with various pitch ratios and revolutions were comprehensively discussed. The computational simulation results are comprehensively presented in Sub-sections 4.1 ~ 4.2.

4.1 Various pitch ratios (P/D) on propeller performance

The negative sign (-) indicates that the CFD result is below the experimental result. The propeller's performance is illustrated through torque (K_Q), thrust (K_T), and efficiency (η) coefficients in Figure 7. Both torque and thrust coefficients gradually decrease with the advancement of the ratio from $J = 0.10$ to 1.3. This decline can be attributed to the reduction in drag force on the blade surfaces. Specifically, the red color contour on the pressure side surface at $J = 0.10$ decreases, reaching a minimum at $J = 0.8$ and 1.0 (refer to Fig. 5) (Nakisa et al., 2013). However, the efficiency coefficient levels off after reaching its maximum point, owing to the reduction of the dark blue contour region on the pressure side and its expansion on the suction side, as depicted in Fig. 6. Moreover, the notable alteration in fluid velocity at high advance ratios influences the increase in the dark blue contour region surrounding the propeller blade (Bicer and Uchida, 2013).

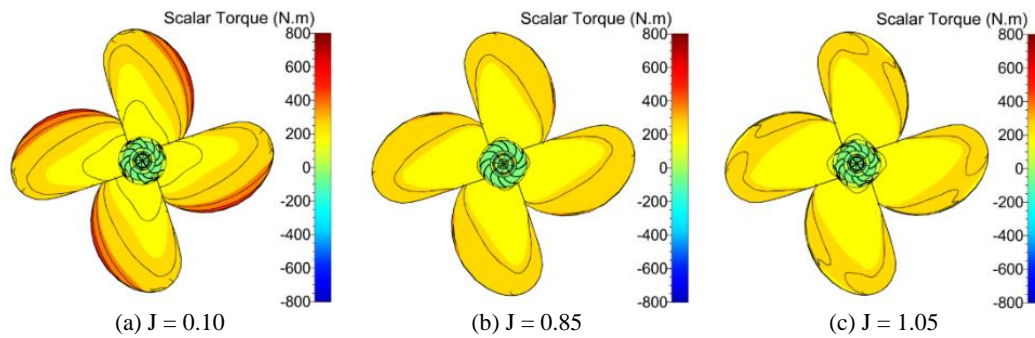


Fig. 5: Scalar torque for 1200 RPM at various advanced ratios, (a) J = 0.10, (b) J = 0.85 and (c) J = 1.05

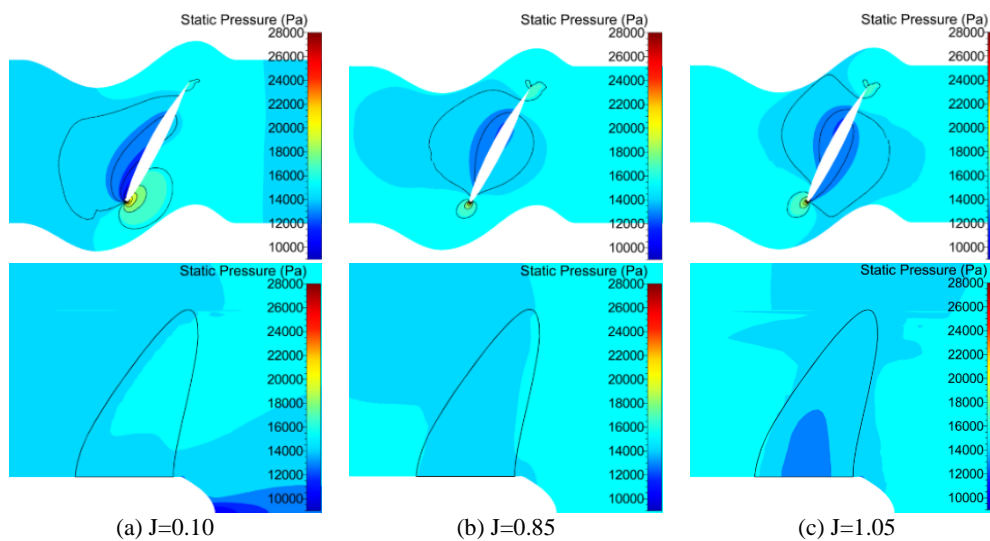


Fig. 6: Blade sectional view (top) and meridional (bottom) views of static pressure for 1200 RPM at (a) J = 0.10, (b) J = 0.85 and (c) J = 1.05

The computational simulation results show the subsequent increase of pitch ratio from $P/D = 0.6$ up to 1.3 was proportional influence the torque and thrust coefficients (refer Table 5 and 6). This aligns with the findings as reported by Bicer and Uchida (2013) and Abdou and Al-Obaidi (2018), the red-orange contour region indicates large amount of scalar torque clearly present as increased the pitch ratio especially at $P/D = 1.3$ as displayed in Fig. 8. This phenomenon possibly occurred due to the increase in area blade surface that is contact with the fluid flow during their operation. The drag force on the blade surface generated at higher pitch ratio required large amount torque value to rotate the propeller and achieved the desired rotational speed. This is relatively affecting the velocity change of fluid flow and static pressure at suction and pressure surfaces. Basically, the rise in thrust coefficient can be attributed to the existence of low static pressure, indicated by the lighter blue contour region, along the blade's pressure side. This increase is inversely proportional to the suction side of the propeller blade surface (refer to Fig. 9), a phenomenon also observed by Abdou and A-Obaidi (2018) and Cong, Loi and He (2018).

In general, the subsequent increase of pitch ratio will increase the overall static pressure surrounding the blade surface. Table 7 showed that the highest efficiency reached a maximum efficiency of 81.2% at $P/D = 1.3$ with $J = 1.15$. Meanwhile, the propeller associated with low pitch ratio has produced highest efficiency at low advance ratio. Merely, it can be inferred from this that the subsequent increase in the pitch ratio predominantly influenced the propeller's performance, as indicated by a noteworthy improvement in propeller efficiency.

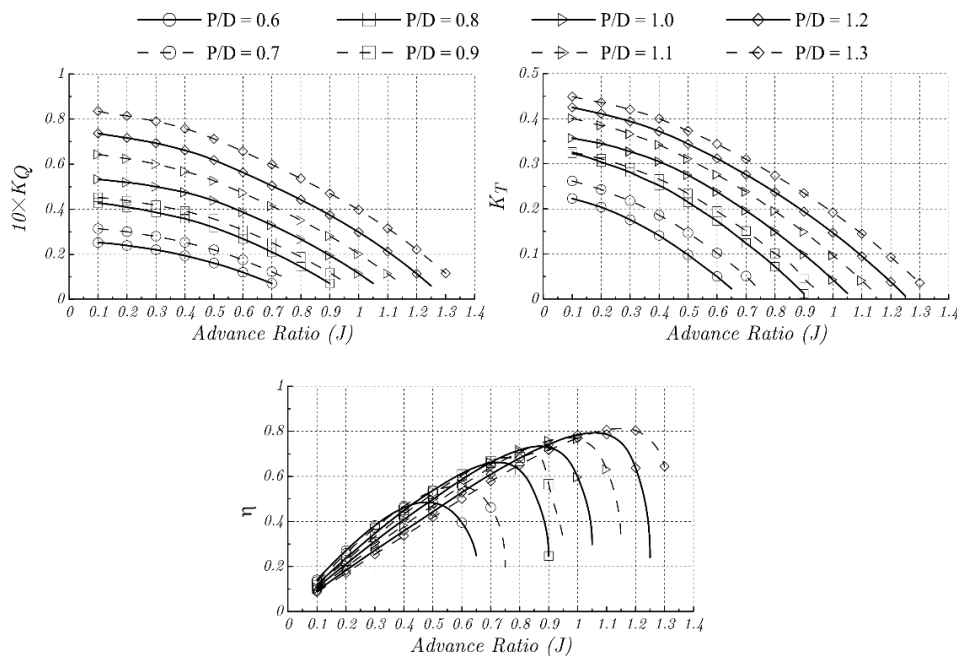


Fig. 7: K_T , $10K_Q$ and η of the propeller at various pitch ratios versus advanced ratio for RPM = 1200 and $Z = 4$

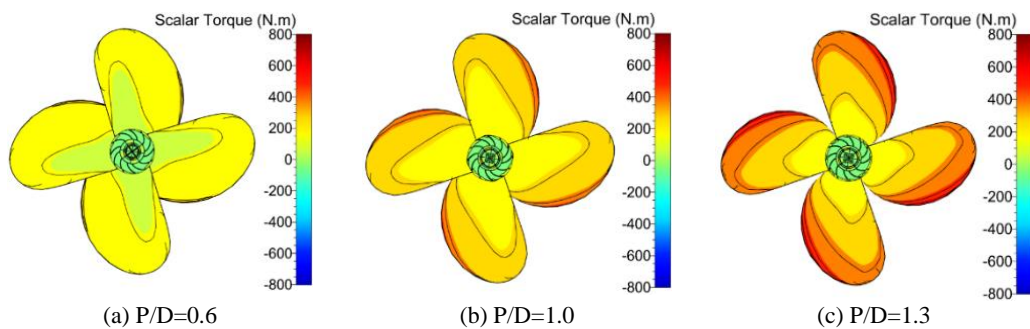


Fig. 8: Scalar torque at various pitch ratios at $J = 0.50$ for (a) $P/D = 0.6$, (b) $P/D = 1.0$ and (c) $P/D = 1.3$

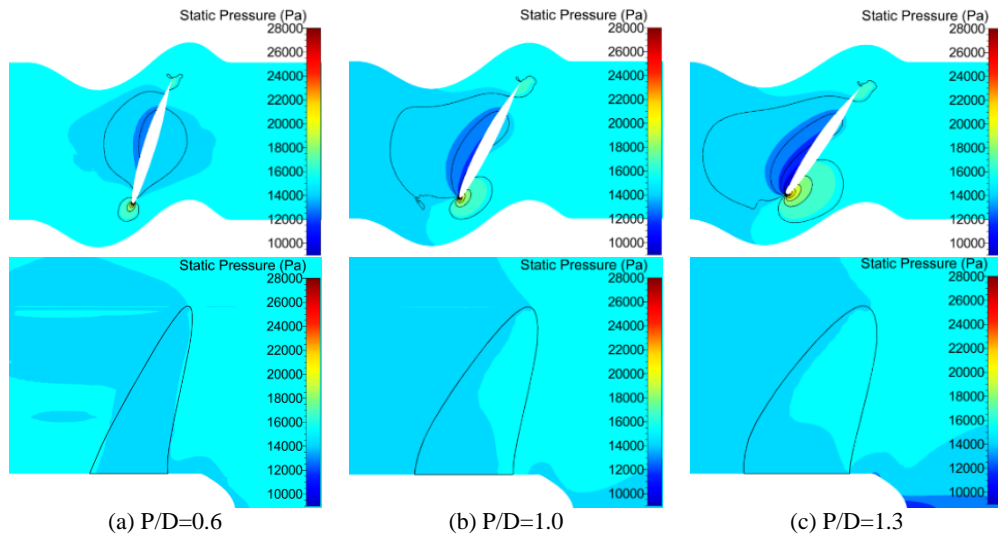


Fig. 9: Blade to Blade (top) and meridional (bottom) views with static pressure at $J=0.50$ for (a) $P/D = 0.6$, (b) $P/D = 1.0$ and (c) $P/D = 1.3$

Table 5: Torque coefficient (K_Q) at various pitch ratios (P/D)

J	Pitch Ratio (P/D)							
	0.6	0.7	0.8	0.9	1.0	1.1	1.2	1.3
0.10	0.252	0.314	0.428	0.453	0.533	0.643	0.736	0.835
0.15	0.247	0.307	0.420	0.446	0.526	0.634	0.726	0.822
0.20	0.239	0.300	0.409	0.438	0.519	0.624	0.716	0.814
0.25	0.230	0.289	0.399	0.428	0.511	0.613	0.705	0.802
0.30	0.220	0.280	0.386	0.418	0.500	0.600	0.693	0.790
0.35	0.208	0.267	0.372	0.405	0.488	0.585	0.678	0.775
0.40	0.194	0.253	0.358	0.392	0.475	0.568	0.661	0.757
0.45	0.178	0.237	0.340	0.375	0.458	0.549	0.642	0.737
0.50	0.161	0.220	0.319	0.357	0.438	0.526	0.618	0.712
0.55	0.142	0.199	0.295	0.333	0.414	0.499	0.591	0.685
0.60	0.120	0.175	0.269	0.308	0.387	0.472	0.563	0.657
0.65	0.096	0.149	0.241	0.281	0.359	0.443	0.534	0.627
0.70	0.071	0.123	0.210	0.252	0.330	0.414	0.504	0.598
0.75	-	0.093	0.179	0.221	0.299	0.383	0.474	0.567
0.80	-	-	0.145	0.189	0.267	0.351	0.442	0.536
0.85	-	-	0.109	0.154	0.232	0.317	0.409	0.503
0.90	-	-	0.071	0.118	0.195	0.281	0.374	0.470
0.95	-	-	-	0.078	0.157	0.243	0.337	0.434
1.00	-	-	-	-	0.115	0.202	0.298	0.397
1.05	-	-	-	-	0.071	0.159	0.257	0.357
1.10	-	-	-	-	-	0.114	0.212	0.315
1.15	-	-	-	-	-	0.065	0.165	0.270
1.20	-	-	-	-	-	-	0.114	0.221
1.25	-	-	-	-	-	-	0.060	0.170
1.30	-	-	-	-	-	-	-	0.116

Table 6: Thrust coefficient (K_T) at various pitch ratios (P/D)

J	Pitch Ratio (P/D)							
	0.6	0.7	0.8	0.9	1.0	1.1	1.2	1.3
0.10	0.223	0.262	0.323	0.326	0.357	0.401	0.425	0.449
0.15	0.214	0.253	0.315	0.319	0.351	0.393	0.418	0.442
0.20	0.204	0.243	0.304	0.311	0.345	0.385	0.411	0.436
0.25	0.191	0.230	0.293	0.302	0.337	0.377	0.403	0.429
0.30	0.176	0.218	0.281	0.291	0.327	0.366	0.394	0.420
0.35	0.159	0.203	0.266	0.279	0.317	0.355	0.384	0.411
0.40	0.141	0.186	0.252	0.266	0.305	0.342	0.372	0.400
0.45	0.120	0.168	0.235	0.251	0.291	0.327	0.359	0.387
0.50	0.098	0.147	0.215	0.234	0.275	0.311	0.344	0.373
0.55	0.074	0.125	0.194	0.215	0.257	0.294	0.328	0.359
0.60	0.050	0.102	0.173	0.195	0.238	0.276	0.312	0.344
0.65	0.023	0.077	0.149	0.173	0.217	0.257	0.294	0.327
0.70	-	0.051	0.124	0.151	0.196	0.238	0.276	0.310
0.75	-	0.015	0.099	0.127	0.174	0.217	0.257	0.293
0.80	-	-	0.072	0.101	0.150	0.195	0.237	0.274
0.85	-	-	0.043	0.080	0.125	0.172	0.216	0.255
0.90	-	-	0.012	0.046	0.099	0.149	0.194	0.235
0.95	-	-	-	0.017	0.072	0.124	0.171	0.214
1.00	-	-	-	-	0.043	0.097	0.147	0.192
1.05	-	-	-	-	0.013	0.070	0.122	0.169
1.10	-	-	-	-	-	0.041	0.095	0.145
1.15	-	-	-	-	-	0.010	0.067	0.120
1.20	-	-	-	-	-	-	0.038	0.093
1.25	-	-	-	-	-	-	0.007	0.065
1.30	-	-	-	-	-	-	-	0.036

Table 7: Propeller efficiency (η) at various pitch ratios (P/D)

J	Pitch Ratio (P/D)							
	0.6	0.7	0.8	0.9	1.0	1.1	1.2	1.3
0.10	0.141	0.133	0.120	0.115	0.107	0.099	0.092	0.086
0.15	0.208	0.196	0.179	0.171	0.159	0.148	0.138	0.128
0.20	0.271	0.258	0.237	0.226	0.211	0.197	0.183	0.171
0.25	0.329	0.317	0.292	0.280	0.262	0.245	0.228	0.213
0.30	0.382	0.372	0.347	0.332	0.312	0.292	0.272	0.254
0.35	0.427	0.422	0.399	0.383	0.361	0.338	0.315	0.295
0.40	0.461	0.468	0.449	0.432	0.408	0.383	0.358	0.336
0.45	0.482	0.506	0.495	0.478	0.454	0.427	0.400	0.376
0.50	0.483	0.534	0.537	0.522	0.498	0.471	0.443	0.417
0.55	0.459	0.552	0.577	0.565	0.543	0.516	0.486	0.459
0.60	0.395	0.557	0.613	0.605	0.586	0.559	0.528	0.500
0.65	0.249	0.533	0.642	0.639	0.626	0.600	0.570	0.540
0.70	-	0.462	0.658	0.667	0.662	0.640	0.609	0.578

0.75	-	0.198	0.659	0.683	0.693	0.676	0.646	0.616
0.80	-	-	0.627	0.684	0.717	0.708	0.681	0.651
0.85	-	-	0.528	0.702	0.732	0.736	0.714	0.685
0.90	-	-	0.247	0.565	0.729	0.758	0.741	0.716
0.95	-	-	-	0.321	0.696	0.771	0.767	0.744
1.00	-	-	-	-	0.596	0.766	0.784	0.770
1.05	-	-	-	-	0.298	0.733	0.793	0.791
1.10	-	-	-	-	-	0.631	0.786	0.806
1.15	-	-	-	-	-	0.295	0.749	0.812
1.20	-	-	-	-	-	-	0.637	0.803
1.25	-	-	-	-	-	-	0.240	0.762
1.30	-	-	-	-	-	-	-	0.644

4.2 Different blade number (Z) on propeller performance

Referring to Figure 10, three different blade numbers are considered with a constant advance ratio ($J = 0.5$). This study wanted to consider the various pitch ratios within the range $0.6 \leq P/D \leq 1.3$. The computation results of three bladed numbers ($Z = 3$) have been revealed that the pitch ratio rises, both thrust and torque coefficients exhibit an upward trend. Similar to what was reported by Abdou and Al-Obaidi (2018), with an increase in the pitch ratio, there is a concurrent increase in pressure applied to the blade surfaces. This occurred due to the increase in the surface area in contact with the fluid which has led to increased pressure on blade at pressure side, where in accordance with thrust and torque generated. Nevertheless, this resulted in a decrease in propeller efficiency for $P/D \geq 0.7$. Irrespective of various pitch ratios, it is worth noting that the propeller with $Z = 3$ exhibited the highest efficiency at 61.9% ($P/D = 0.7$) compared to $Z = 4$ and $Z = 5$. This can be attributed to the expansion of the lower-pressure area (dark blue contour region) around the blades, predominantly leading to a reduction in propeller efficiency, as illustrated in Figures 12 (a), (b), and (c) (Yeo and Hau, 2014). Additionally, the subsequent increase in blade numbers significantly raised thrust and torque coefficients. This might be attributed to the raising in the overall surface area of the blades, leading to a proportionally increased drag force, as evidenced by the orange contour region surrounding the blades. (see Fig. 11).

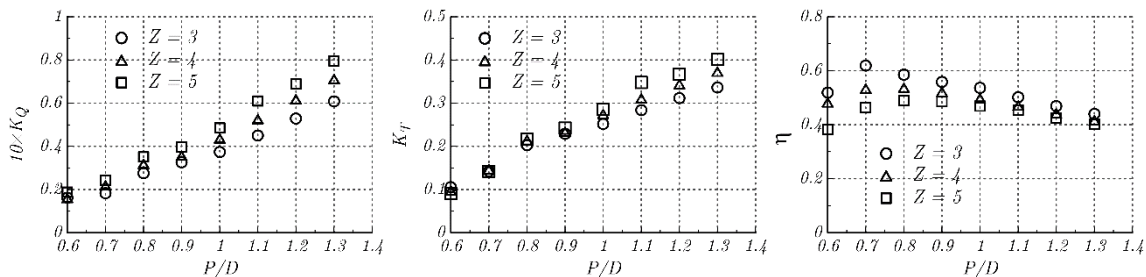


Fig. 10: K_T , $10K_Q$ and η coefficients of the propeller at various blade numbers versus P/D

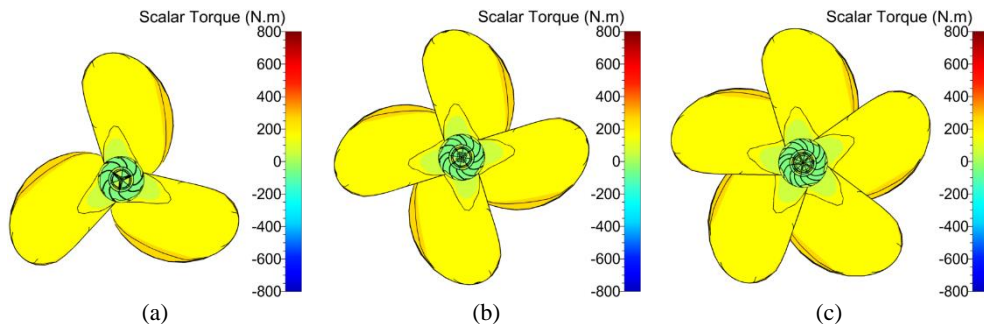


Fig. 11: Scalar torque contour for side pressure at (a) $Z = 3$, (b) $Z = 4$ and (c) $Z = 5$ for $P/D = 0.7$

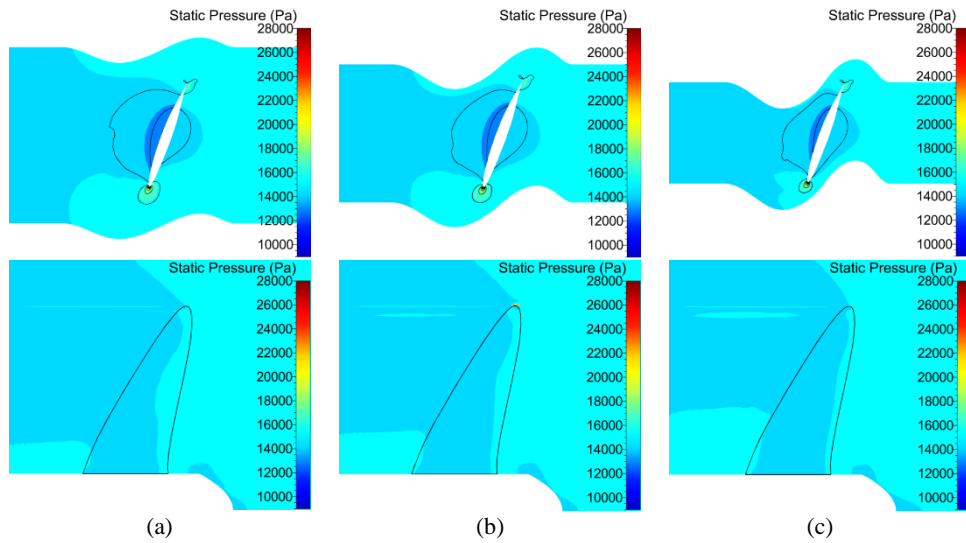


Fig. 12: Blade to Blade (top) and meridional (bottom) views of static pressure contour around the blades surface at (a) $Z = 3$, (b) $Z = 4$ and (c) $Z = 5$ for $P/D = 0.7$

Table 8: Torque, thrust and efficiency coefficients of propeller at various propeller revolutions

P/D	Z = 3			Z = 4			Z = 5		
	10K _Q	K _T	η	10K _Q	K _T	η	10K _Q	K _T	η
0.6	0.162	0.106	0.519	0.161	0.098	0.483	0.188	0.090	0.382
0.7	0.183	0.142	0.619	0.220	0.147	0.534	0.244	0.142	0.464
0.8	0.276	0.203	0.586	0.319	0.215	0.537	0.351	0.216	0.490
0.9	0.326	0.229	0.559	0.357	0.234	0.522	0.397	0.242	0.485
1.0	0.373	0.252	0.536	0.437	0.275	0.498	0.485	0.286	0.469
1.1	0.450	0.284	0.502	0.526	0.311	0.471	0.610	0.348	0.454
1.2	0.529	0.312	0.469	0.618	0.344	0.443	0.689	0.367	0.424
1.3	0.608	0.336	0.440	0.712	0.373	0.417	0.795	0.401	0.401

In general, K_T , K_Q and η values generally increase as blade numbers decrease; meanwhile, the propeller typically attains maximum efficiency in the $0.7 \leq J \leq 0.8$ range, irrespective of the specific blade number.

5. Conclusions

The computational simulation accurately predicted the characteristics of the B-series propeller in open-water conditions, considering various pitch ratios (P/D) and blade numbers (Z) with different advances. The characteristics of the torque, thrust and efficiency coefficients were evidently investigated. The results can be merely written as follow:

- The increase of the propeller pitch ratio is proportional to the thrust and efficiency coefficients, where the maximum pitch ratio ($P/D = 1.3$) produces the highest efficiency coefficient by 81.2%. The explanation lies in the fact that the increase in pitch ratio has a more significant effect on torque and static pressure increments compared to blade number.
- Regardless of pitch ratios, an inherent decrease in propeller's performance occurs with an increase in propeller blade numbers, resulting in lower efficiency, particularly at $P/D \geq 0.7$. This is possibly due to the increase in overall blade surface area, resulting in a proportionately higher drag force.

Acknowledgement

The authors wish to extend sincere thanks to P.T. Terafulk Megantara Design and Numit Enterprise for their valuable collaboration in this research.

References

Dymarski, C. (2008). Research on a control system based on stepping motor for ship's controllable pitch propellers. Polish Maritime Research, 15(1), 37-41. <http://dx.doi.org/10.2478/v10012-007-0049-2>

- Bacciaglia, A., Ceruti, A., and Liverani, A. (2021). Controllable pitch propeller optimization through meta-heuristic algorithm. *Engineering with Computers*, 37, 2257-2271. <http://dx.doi.org/10.1007/s00366-020-00938-8>
- Yousefi, A., Shafaghat, R., Beykani, M., Aghajani Afghan, A., and Seyyed Mostafa, S. T. (2023). Experimental study to investigate effect of pitch ratio and number of blades on hydrodynamic performance of surface piercing propellers. *Iranian (Iranica) Journal of Energy and Environment*, 14(1), 26-37. <http://dx.doi.org/10.5829/IJEE.2023.14.01.04>
- Rahman, A., Ullah, M. R., and Karim, M. M. (2017). Marine propeller design method based on lifting line theory and lifting surface correction factors. *Procedia engineering*, 194, 174-181. <http://dx.doi.org/10.1016/j.proeng.2017.08.132>
- Abbasi, A., Ghassemi, H., and Fadavie, M. (2018). Hydrodynamic characteristic of the marine propeller in the oblique flow with various current angle by cfd solver. *American Journal of Marine Science*, 6(1), 25-29.
- Mao, Y., and Young, Y. L. (2016). Influence of skew on the added mass and damping characteristics of marine propellers. *Ocean Engineering*, 121, 437-452. <http://dx.doi.org/10.1016/j.oceaneng.2016.05.046>
- Kang, J. G., Kim, M. C., Kim, H. U., and Shin, I. R. (2019). Study on propulsion performance by varying rake distribution at the propeller tip. *Journal of Marine Science and Engineering*, 7(11), 386. <http://dx.doi.org/10.3390/jmse7110386>
- Adam, N. A., Fitriadhy, A., Quah, C. J., and Haryanto, T. (2020). Computational analysis on B-series propeller performance in open water. *marine systems and ocean technology*, 15(4), 299-307. <http://dx.doi.org/10.1007/s40868-020-00087-z>
- Prakash, S., and Nath, D. R. (2012). A computational method for determination of open water performance of a marine propeller. *International Journal of Computer Applications*, 58(12).
- Deck, S., Duveau, P., d'Espiney, P., and Guillen, P. (2002). Development and application of Spalart–Allmaras one equation turbulence model to three-dimensional supersonic complex configurations. *Aerospace Science and Technology*, 6(3), 171-183. [http://dx.doi.org/10.1016/S1270-9638\(02\)01148-3](http://dx.doi.org/10.1016/S1270-9638(02)01148-3)
- Lorin, E., Ali, A. B. H., and Soulaïmani, A. (2006, September). An accurate positivity preserving scheme for the spalart-allmaras turbulence model. In *Application to aerodynamics*, Presented at the 36th AIAA Fluid Dynamics Conference and Exhibit. <http://dx.doi.org/10.2514/6.2006-3743>
- Hejlesen, M. M., Rasmussen, J. T., Larsen, A., and Walther, J. H. (2012). Implementation of the Spalart-Allmaras turbulence model in the two-dimensional vortex-in-cell method. 6th European Congress on Computational Methods in Applied Sciences and Engineering, Vienna, Austria.
- Kostić, Č. (2015). Review of the Spalart-Allmaras turbulence model and its modifications to three-dimensional supersonic configurations. *Scientific Technical Review*, 65(1), 43-49.
- International, N., FINE/Turbo v8. 7, User Manual. 2009, NUMECA International Brussels.
- Gerr, D. (1989). *Propeller handbook*. International Marine Publishing.
- Ozturk, D., Delen, C., Belhenniche, S. E., and Kinaci, O. K. (2022). The effect of propeller pitch on ship propulsion. *Transactions on Maritime Science*, 11(01), 0-0. <http://dx.doi.org/10.7225/toms.v11.n01.w09>
- Colley, E. (2012). Analysis of flow around a ship propeller using OpenFOAM. Curtin University, October.
- Martinez, J. A. V. I. E. R., Doerffer, P., Szulc, O., and Tejero, F. (2015). Aerodynamic analysis of wind turbine rotor blades. *Task Quarterly*, 19(2), 129-140.
- Kamal, I. M., and Yusof, T. M. A. T. M. (2017). A CFD RANS cavitation prediction for propellers.
- Folkner, D. E. (2013). Improvement in computational fluid dynamics through boundary verification and preconditioning. Utah State University.
- ITTC (2017). Recommended procedure and guidelines: uncertainty analysis in CFD verification and validation methodology and procedure, International Towing Tank Conference.
- Wald, Q. R. (2006). The Aerodynamics of propellers. *Progress in Aerospace Sciences*, 42(2), 85-128. <http://dx.doi.org/10.1016/j.paerosci.2006.04.001>
- Nakisa, M., Maimun, A., Ahmed, Y. M., and Behrouzi, F. (2013, December). Numerical analysis of three-dimensional flow around marine propellers in restricted water. *IOP Conference Series: Materials Science and Engineering* (Vol. 50, No. 1, p. 012046). IOP Publishing. <http://dx.doi.org/10.1088/1757-899X/50/1/012046>
- Bicer, B., and Uchida, M. (2013). Numerical performance investigations of screw propellers by lifting surface theory. *Marine Engineering*, 48(2), 246-252. <http://dx.doi.org/10.5988/jime.48.246>
- Abdou, M., and Al-Obaidi, A. S. M. (2018). Studying the effect of pitch ratio on sheet cavitation in marine propellers. *Journal of Engineering Science and Technology*, 13, 28-38.
- Cong, N. C., Loi, L. N., and Van He, N. (2018). A study on effects of blade pitch on the hydrodynamic performances of a propeller by using CFD. *Journal of Shipping and Ocean Engineering*, 8, 36-42. <http://dx.doi.org/10.17265/2159-5879/2018.01.005>
- Yeo, K. B., and Hau, W. Y. (2014). Fundamentals of marine propeller analysis. *Journal of Applied Sciences*, 14(10), 1078-1082. <http://dx.doi.org/10.3923/jas.2014.1078.1082>